Modelling and
Simulation in Materials
Science and
Engineering

PURPOSE-LED
PUBLISHING™

PAPER

MD assessment of irradiation resistance of FeMnNiCr under successive bombardment

To cite this article: Chengyue Xiong *et al* 2025 *Modelling Simul. Mater. Sci. Eng.* **33** 025023

View the article online for updates and enhancements.

You may also like

- A non-isothermal phase-field crystal model with lattice expansion: analysis and benchmarks
Maik Punke, Marco Salvalaglio, Axel Voigt et al.
- *Ab initio* computational study of hydration thermodynamics in cubic yttria-stabilized zirconia
A G Marinopoulos
- Effect of anisotropic Peierls barrier on the evolution of discrete dislocation networks in Ni
John D Shimanek, Darshan Bamney, Laurent Capolungo et al.

This content was downloaded from IP address 58.48.207.61 on 29/12/2025 at 07:48

IOP Publishing Modelling and Simulation in Materials Science and Engineering

Modelling Simul. Mater. Sci. Eng. **33** (2025) 025023 (15pp) https://doi.org/10.1088/1361-651X/adafc7

MD assessment of irradiation resistance of FeMnNiCr under successive bombardment

Chengyue Xiong[1,2], Lei Guo[3], Zunhao Liu[3], Rui Li[3,*] and Qing Peng[4,5,6,*]

[1] Beijing National Innovation Institute of Lightweight Ltd, Beijing 101400, People's Republic of China
[2] State Key Laboratory of Advanced Forming Technology and Equipment, China Academy of Machinery Science & Technology, Beijing 100044, People's Republic of China
[3] School of Mechanical Engineering, University of Science and Technology Beijing, Beijing 100083, People's Republic of China
[4] State Key Laboratory of Nonlinear Mechanics, Institute of Mechanics, Chinese Academy of Sciences, Beijing 100190, People's Republic of China
[5] Center of Materials Science and Optoelectronics Engineering, University of Chinese Academy of Sciences, Beijing 100049, People's Republic of China
[6] Guangdong Aerospace Research Academy, Guangzhou 511458, People's Republic of China

E-mail: lirui@ustb.edu.cn and pengqing@imech.ac.cn

Received 3 September 2024; revised 9 December 2024
Accepted for publication 29 January 2025
Published 14 February 2025

Abstract

The irradiation resistance behavior of Co-free high-entropy alloy FeMnNiCr under successive bombardment is investigated by means of molecular dynamics simulations. There are much less residual defects in FeMnNiCr referring to Ni after prolonged irradiation and large-size defect clusters are observed in FCC Ni but not FeMnNiCr. The formation and growth of dislocations in FeMnNiCr are significantly suppressed. The migration barriers of interstitials are similar to these of vacancies in FeMnNiCr, resulting in a higher efficiency of defect recombination. The defects in Co-free FeMnNiCr show similar trends with NiCoCrFeMn and NiCoCrFe during the irradiation process, suggesting its good potential in nuclear structure materials applications.

Keywords: high entropy alloys, irradiation resistance, successive bombardment, molecular dynamics

* Authors to whom any correspondence should be addressed.

© 2025 IOP Publishing Ltd.
All rights, including for text and data mining, AI training, and similar technologies, are reserved.

1. Introduction

With the rising demand for efficient and clean energy, it has become crucial to explore advanced nuclear energy systems with high safety and competitiveness [1–4]. High irradiation resistance materials is desirable for the applications in structural materials in nuclear energy [5]. In recent years, one kind of novel solid solution alloy materials high entropy alloys (HEAs) has attracted extensive attention [6, 7]. Unlike traditional alloys that typically have one or two major elements, HEAs are composed of multiple primary elements in nearly equal atomic ratios. This new class of alloy designs has generated a great deal of interest among researchers due to the excellent material properties of HEAs [8–11]. Researchers have demonstrated that HEAs had excellent anti-irradiation properties [12–14], making them promising candidates for next-generation nuclear structural materials [15, 16]. For example, researchers have experimentally investigated the irradiation resistance of high-entropy alloys. Lu *et al* [16] compared the defect evolution behavior of one- to five-elements alloys under Ni ion irradiation at various irradiation doses at 773 K, resulting that NiCoFeCrMn exhibited smaller pore sizes with the increase of the number of elements. Zhang *et al* [17] found that HEA FeCrNiCoMn showed very low swelling rates under high-energy Au ion irradiation, and no nanocrystal precipitation was observed, proving its good microstructural stability. Abhaya *et al* [18] indicated that HEA NiCoFeCr did not exhibit phase separation or precipitation of a second phase even under 100 displacements per atom irradiation.

Because the changes in the atomic-level microstructure after irradiation is difficult to observe in experiments, the effective method to evaluate their properties is to examine defect generation and microstructural evolution following irradiation by atomistic simulations [19, 20]. Researchers have carried out extensive simulation studies on the micro-mechanisms of HEA against irradiation [21–23]. For example, Lin *et al* [24] conducted displacement cascade simulations of NiCoFeCr HEAs. The results showed that the alloys exhibit prolonged thermal peaks and a higher recombination rate of defects due to their low thermal conductivity. Do and Lee [25] carried out cascade simulations for CoCrFeMnNi and found that the clusters of larger size defects are unstable due to the complexity of the alloy. Most of these atomistic simulations are for single displacement cascade event.

However, single displacement cascade simulation of irradiation resistance behavior has limitations, which cannot fully capture the long-term irradiation behavior of structural materials. For example, successive bombardment simulations of Ni and Ni-based alloys showed [26] that the growth of large defect clusters in Ni-based alloys is slower compared to Ni, although the number of point defects produced in a single cascade is close for different materials. Similarly, successive bombardment simulations of SiC by Gao and Weber [27] unveiled irradiation-induced amorphization, a phenomenon absent in single displacement cascade. The irradiation behavior under successive bombardment is significantly different from that of single displacement cascades. Thus it is necessary to investigate the behavior of HEAs under prolonged irradiation. In addition, it is important to examine the elemental compositions of widely investigated high-entropy alloys (CoCrFeMnNi [12, 13], NiCoFeCr [28, 29], NiCoFeCrAl [30, 31], etc) for the practical applications as nuclear structural materials. The efforts include the long decay time of Co element after irradiation [32], which may increase the potential risk during maintenance and is not suitable for use as a structural material in nuclear reactors [10, 33]. Recently, a Co-free high-entropy alloy, FeMnNiCr [32, 34–36], has been widely studied, however, the microscopic mechanism of its resistance to long-term irradiation is still not fully understood yet. It is desirable to investigate its defect evolution behavior after successive irradiation.

In this study, we employ molecular dynamics (MD) simulations to investigate the irradiation resistance behavior of equiatomic FeMnNiCr HEA under long-time irradiation at 600 K, aiming to elucidate the influence of alloy complexity of FeMnNiCr on defect evolution and dislocation behavior. The irradiation behavior of FeMnNiCr (Co-free) is compared with that of CoCrFeNiMn and CoCrFeNi (with Co) to verify its irradiation performance. This study might provide theoretical insights for the practical application of FeMnNiCr in nuclear structural materials.

2. Methodology

We simulate the anti-irradiation behavior of FeMnNiCr and Ni under continuous irradiation conditions by the MDs simulations employed as the software LAMMPS [37]. As shown in figure 1, the size of Ni and FeMnNiCr is set to $25a_0 \times 25a_0 \times 25a_0$, ($a_0$ is the lattice constant of the FCC lattice) containing 62 500 atoms. The four elements of FeMnNiCr are randomly distributed. The lattice constant a_0 is 0.3552 and 0.352 nm for FeMnNiCr and Ni, respectively. The boundary conditions are set to be periodic in the *X, Y*, and *Z* directions. Before the cascade bombardment simulation, the system relaxes with isothermal–isobaric (NPT) ensemble at a temperature of 600 K for 10 ps, leading to a thermodynamical equilibrium. Berendsen thermal bath is applied at 600 K to 1 nm-thick layer on the boundary of model in order to eliminate the heat generated during the cascade process.

The primary knock-on atoms (PKA) for each bombardment are randomly selected from the center region of the model and given an initial energy of 3 keV to trigger the cascade collisions in a random direction. Each bombardment simulation lasts for 20 ps and uses an adaptive time step to ensure that the atoms produce a displacement of no more than 0.002 nm per time step. The simulation is performed for 400 consecutive bombardments. This model is dynamically shifted after each bombardment to ensure that the cascade is always produced in the central region to reduce the boundary effect.

MEAM potential developed by Choi *et al* [38] is chosen for both FeMnNiCr and Ni models in order to compare their irradiation resistance behavior, which has been widely demonstrated to be effective in simulating the irradiation properties of CoCrFeNiMn high-entropy alloys [25], and the Ziegler-Biersack-Littmark potential function [39] is smoothly connected to the above potential to describe the atomic short-range forces during the collision process.

The open source software OVITO [40] is applied to visualize the formation, evolution and distribution of defects. The centrosymmetry parameter [41] is used to identify interstitial atoms and vacancy defects generated during bombardment process. The dislocation extraction algorithm [42] is applied to recognize dislocations. The common neighbor analysis [43] is applied to observe the change of phase structures in the model.

3. Results and discussions

3.1. Defects evolution

The defect numbers of FeMnNiCr and Ni during successive bombardment is shown in figure 2. In the initial stage of successive bombardment, the number of defects in FeMnNiCr and Ni shows an approximate linear increase. This is a rapid accumulation process of defects, as the displacement cascade mainly occurs inside the crystal without initial defects. When the number

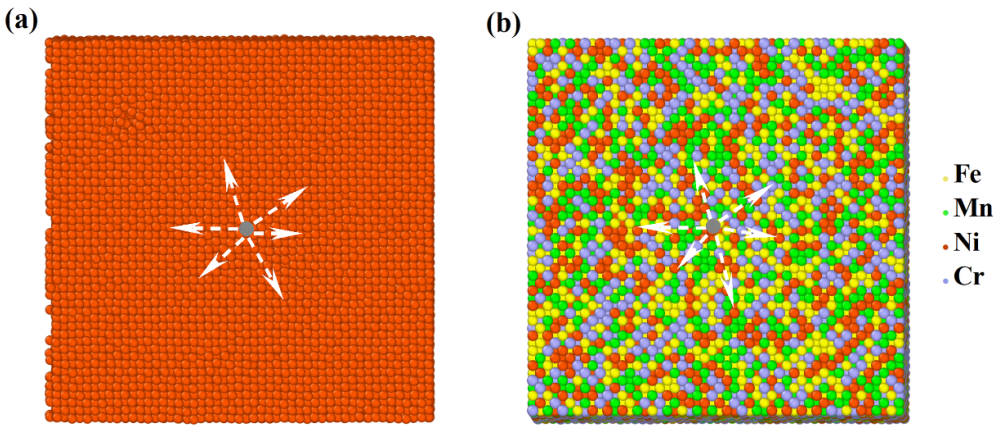

Figure 1. Successive bombardment model: (a) Ni; (b) FeMnNiCr.

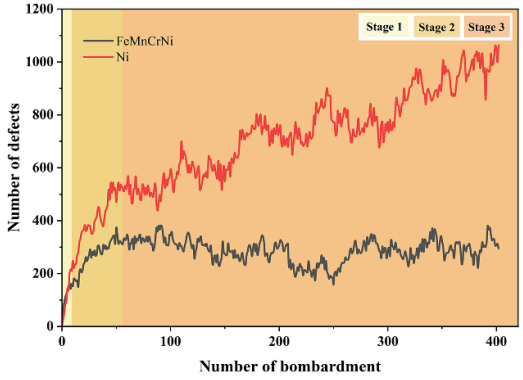

Figure 2. The number of defects in FeMnNiCr and Ni with the number of bombardments.

of bombardments reaches about 10, as shown as stage 2, new displacement cascades may occur in the region with existing defects. At this point, the growth rate of the overall number of defects slows down due to overlapping cascades. In the third stage, When the number of bombardments is larger than 56, as shown as the dark grey region in figure 2, the evolution of defects in the two materials shows different trends. The number of defects in FeMnNiCr tends to saturate and fluctuates around the value of 300. A similar trend was shown in our previous work for CoCrCuFeNi [44]. On the contrary, the number of defects continues to increase following the bombardment process in the case of Ni. At the end of 400th bombardment, the number of defects in FeMnNiCr is only 295, while the defect number of Ni is as high as 1063, which is nearly three times higher than that in FeMnNiCr.

Figure 3 shows the evolution of defect clusters of different sizes in FeMnNiCr and Ni during bombardment process at a temperature of 600 K with $E_{\mathrm{PKA}} = 3$ keV. In figures 3(a) and (b), the number of FeMnNiCr and Ni interstitial clusters of each size is calculated every 100 times of bombardment. The results show that the number of FeMnNiCr and interstitial clusters varies slightly after 100th bombardment, which indicates that the defects in the system are stable.

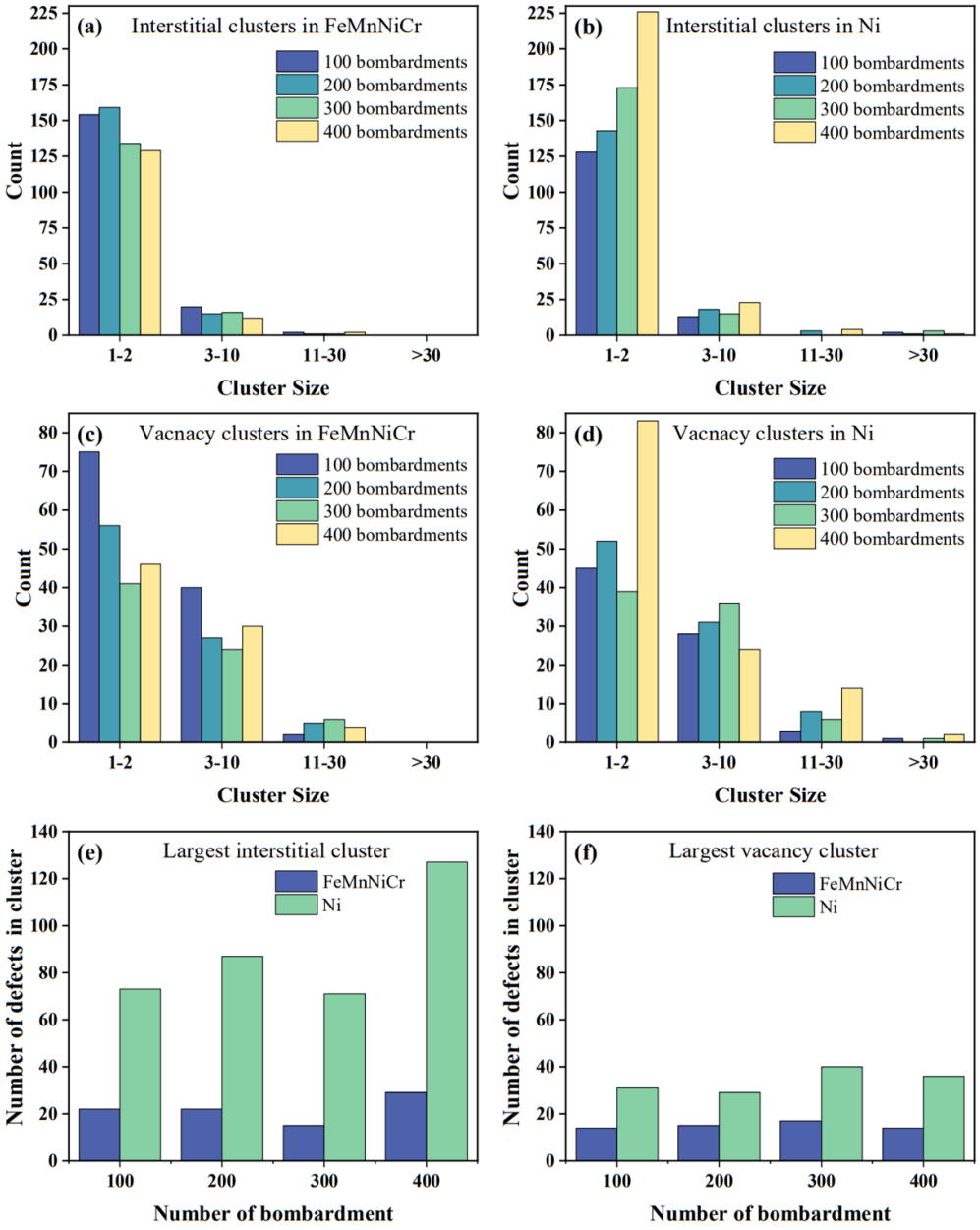

Figure 3. Size distribution of defect clusters in the cascade process: the number of interstitial clusters of different sizes in FeMnNiCr (a) and Ni (b); the number of vacancy clusters of different sizes in FeMnNiCr (c) and Ni (d); (e) the largest size of interstitial cluster in FeMnNiCr and Ni; (f) the largest size of vacancy cluster in FeMnNiCr and Ni.

However, in the case of Ni, new small interstitial clusters containing 1–2 atoms are continuously generated, and a multitude of small interstitial clusters meet and gather together, therefore, the number of interstitial clusters of all sizes shows an upward trend. The large interstitial

clusters containing >30 interstital atoms are formed after 400 bombardments. On the contract, it is not observed in FeMnNiCr. The largest size of interstitial cluster in FeMnNiCr and Ni during the cascade process is shown in figure 3(e). There is only a certain dynamic fluctuation of the maximum interstitial cluster size in FeMnNiCr. However, the size of the largest interstitial cluster in Ni increases gradually. The maximum interstitial cluster size in FeMnNiCr contains 29 interstitial atoms after 400 times of bombardment, whereas the number in Ni reaches 127, which is about 4.4 times of that in FeMnNiCr. In addition, it is evident from figures 3(c) and (d) that vacancy clusters exist mainly as small vacancy clusters and medium-sized clusters in both FeMnNiCr and Ni. Meanwhile, the largest vacancy cluster size in FeMnNiCr is also significantly smaller than that in Ni, as shown in figure 3(f). The results reveal that FeMnNiCr has better irradiation tolerance than Ni under prolonged irradiation.

3.2. Dislocation and phase structure evolution

Under the effect of long-term irradiation, the vacancies and interstitial atoms generated within the material will gradually aggregate to form clusters and further evolve into dislocations. These point defects and the dislocations have significant impact on mechanical properties of the material. The evolution of dislocations has been investigated to deepen the understanding of the anti-irradiation mechanism of FeMnNiCr and Ni under prolonged irradiation conditions. The distribution of point defects and dislocations in FeMnNiCr under different times of bombardment (100–400 times) is shown in figure 4. Only few small size dislocations exist within FeMnNiCr despite the increase of the number of bombardments. The vacancy and interstitial atoms have not formed larger size clusters, which is consistent with the conclusions in section 3.1.

In contrast, the evolution of the dislocation in Ni during irradiation is significantly different, as shown in figure 5, where new dislocation continues to be generated following the bombardments. In particular the $1/3 < 111 >$ Frank dislocation continues to grow as a ring structure, which is in agreement with Levo *et al* [45]. After 400 times of bombardment, stacking fault tetrahedra composed of six $1/6 < 110 >$ Stair-rod dislocations is observed in Ni, indicating that defects in Ni are more prone to migrate and aggregate to form relatively stable dislocation structures, whereas the formation and growth of the dislocations are significantly inhibited in FeMnNiCr.

In order to analyze the detailed evolution of the dislocations, the total length, dislocation density, and average dislocation length of dislocations in FeMnNiCr and Ni are shown in figure 6. Massive dislocations appear in Ni at the early phase of the bombardment as shown in figure 6(b), and the dislocation density rapidly increased to 13×10^{25} m^{-2}. Following the bombardment process, the dislocation density shows large fluctuations. The total length of dislocations rises and reaches a high level in Ni even if there is absorption evolution between dislocations, as shown in figure 6(a). The peak of the average dislocation length in Ni in figure 6(c) may be due to the absorption evolution of $1/3 < 111 >$ Frank dislocations. This absorption leads to the formation of larger size dislocations in the system, resulting in the average dislocation size of the system reaching nearly 12 nm. In contrast, the total dislocation length, dislocation density, and the average dislocation length of FeMnNiCr all maintain at low levels. This result is consistent with the result of Kumar *et al* that only small size dislocations were observed in irradiation experiments of FeMnNiCr at 700 °C [33].

The proportion of FCC phase structure is displayed in figure 7 for FeMnNiCr and Ni during successive bombardment process. The proportion of FCC phase in Ni continues to decrease from the beginning of 100% to 93.46% at the end of the bombardment. In FeMnNiCr, the FCC

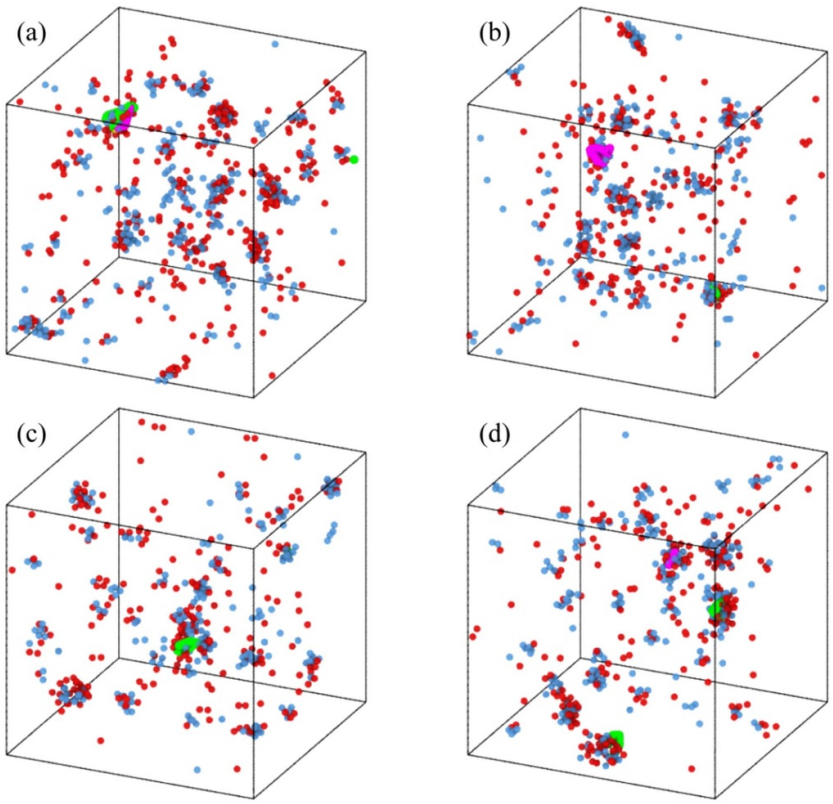

Figure 4. Distribution of point defects and dislocations in FeMnNiCr: (a)∼(d) after 100, 200, 300, and 400 bombardments, respectively. The blue and red atoms represent vacancies and interstitials. Different color lines represent different kinds of dislocation, where green, purple, light blue and pink lines represent 1/6 $<112>$ Shockley dislocation, 1/3 $<111>$ Frank dislocation and 1/6 $<110>$ Stair-rod dislocation, respectively.

phase decreases rapidly at the early stage and reaches stable quickly. At the end of bombardment, the proportion of FCC phase is similar in two materials, However, it is believed the proportion of FCC phase will be lower in Ni than in FeMnNiCr because FCC phase decreases continuously, which implies better phase stability of FeMnNiCr under successive bombardment.

3.3. Defect formation energy

To gain more atomistic insights, we have further examined the defect formation energy in two simulation systems FeMnNiCr and Ni. The model size is $10a_0 \times 10a_0 \times 10a_0$, containing 4000 atoms. In this section, the bombardment processes are not applied to the systems. The defect formation energy is calculated using the same method in the [46]. Since Ni only has one element, formation energy obtained at any point site within the system is equal. However, FeMnNiCr consists of four different types of atoms and each of them is randomly distributed in the crystal lattice, therefore, 10 randomly selected point sites are chosen for each type of atoms, and their defect formation energies are calculated and averaged.

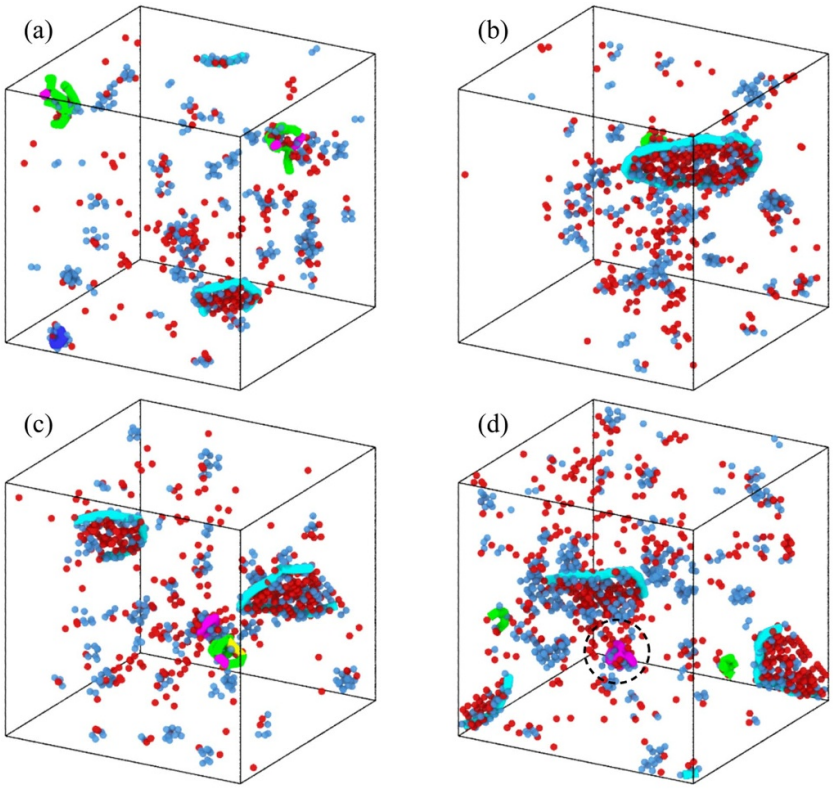

Figure 5. Distribution of point defects and dislocations in Ni: (a)∼(d) after 100, 200, 300, and 400 bombardments, respectively. The structures indicated by the different colors are consistent with figure 4.

The defect formation energies of FeMnNiCr alloy and Ni are shown in figure 8. The interstitial formation energy of each atom in FeMnNiCr is all smaller than that in Ni (figure 8(a)), with an average value of 3.54 eV, while that of Ni is 4.94 eV. Interstitial atoms are more easily generated in FeMnNiCr. In addition, the interstitial formation energies of NiCoCr, NiCoFeCr, and NiCoFeCrCu were also smaller than those of Ni [44, 47]. Moreover, the formation energy of vacancy in FeMnNiCr is also smaller than that in Ni, which implies more defects will be generated at the thermal spike of one PKA simulation. However, the number of residual defects in FeMnNiCr is smaller, as described in section 3.2. The results are consistent with Wang *et al* [48]. In addition, the vacancy formation energies of FeMnNiCr and Ni are smaller than their interstitial formation energies, and thus vacancy defects are more likely to be formed than interstitial atoms.

3.4. Migration energy of defects

Migration modes of point defects plays an important role in residual defects and irradiation resistance properties of materials. To explain why the number of defects in FeMnNiCr is smaller than that in Ni, migration energies of defects are calculated in this section. The simulation models are the same with section 3.3. The migration energy of point defects in the two materials is calculated by the nudged elastic band method [49, 50], in which the initial and final stable

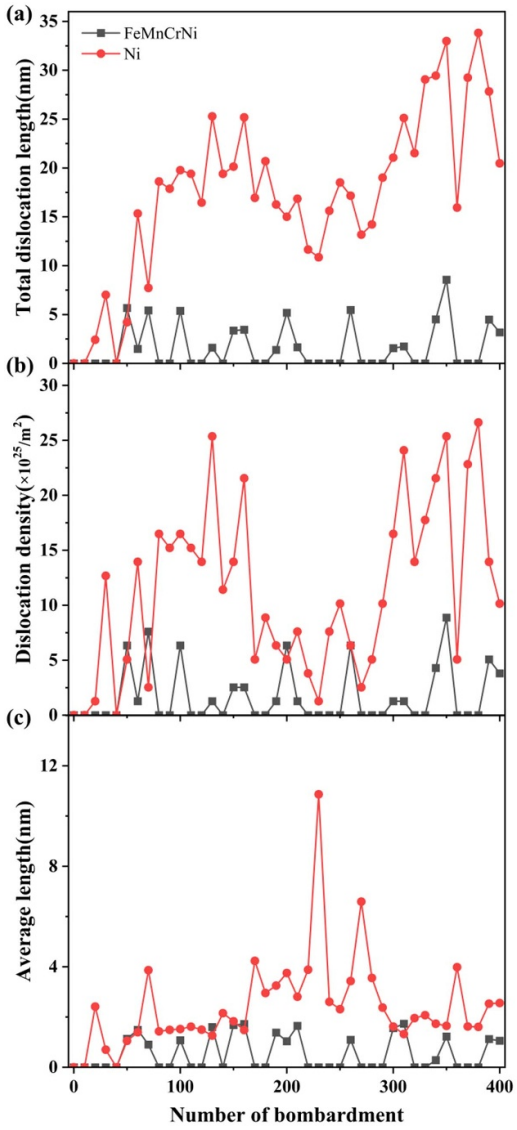

Figure 6. Dislocations of FeMnNiCr and Ni in the cascade process. (a) Total dislocation length. (b) Dislocation density. (c) Average dislocation length.

positions of point defect in the lattice are built and the lowest energy path during migration is searched by iterative optimization. The migration energy of a point defect is defined as the energy barrier to be overcome on the migration path. Considering the random distribution of atoms in FeMnNiCr, we calculate migration energy for 10 times and average the results, are shown in figure 9.

The average migration energy of interstitial atoms in FeMnNiCr is 0.58 eV, while that in Ni is 0.25 eV. The high migration energy proves that interstitial atoms are more difficult to migrate in FeMnNiCr than in Ni, which can be attributed to lattice distortion caused by the random distribution of atoms in FeMnNiCr. The initial energies of PKA atoms are much higher

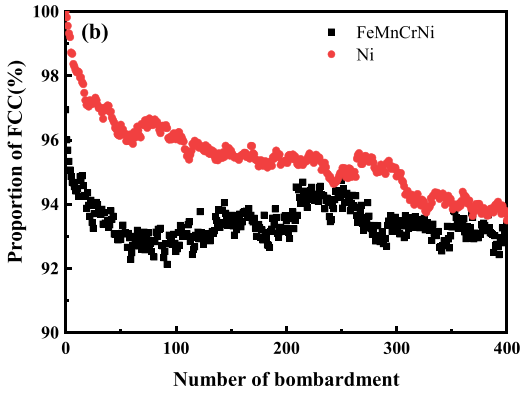

Figure 7. The proportion of FCC phases during successive bombardment of FeMnNiCr and Ni.

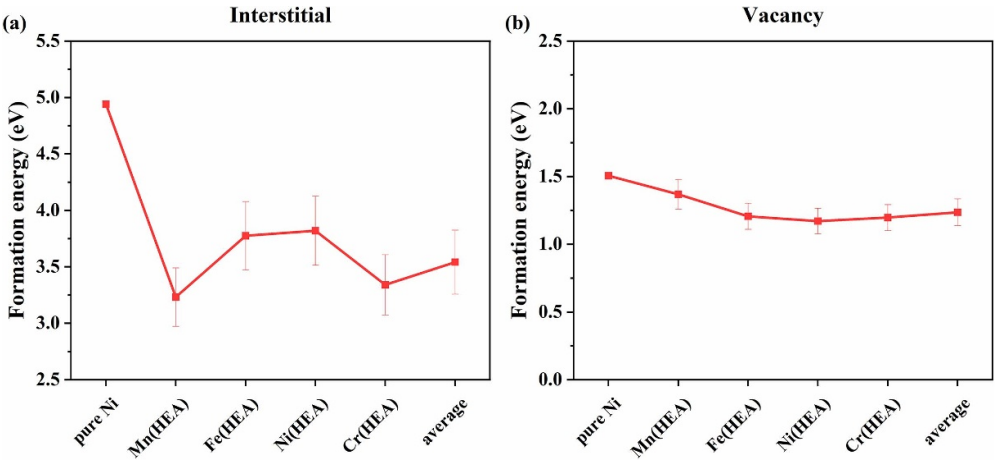

Figure 8. Defect formation energy of FeMnNiCr and Ni. (a) Interstitial. (b) Vacancy.

than the dislocation energy. Therefore, the evolution of the cascade is mainly the movement of the interstitial atoms. Meanwhile, the average migration energy of vacancies in FeMnNiCr is 0.88 eV, which is lower than that of Ni (1.58 eV), indicating that vacancies in FeMnNiCr migrate more easily. Especially the vacancy of Ni elements in pure Ni have the highest migration energies compared to other cases, which suggests that the movement of vacancies in Ni is the most difficult.

Figure 10 shows the difference of the migration energies between interstitial and vacancy defects in FeMnNiCr and Ni. All the values are positive. The difference of each element in FeMnNiCr is smaller than that of Ni. The average difference of migration energies of between interstitial and vacancy defects in FeMnNiCr is only 0.3 eV. Whereas in Ni, this difference value reaches 1.33 eV, which implies that the defects in FeMnNiCr exhibit more similar migration properties. Therefore, larger overlap region of interstitials and vacancies are obtained in FeMnNiCr. The previous study on tungsten-containing high-entropy alloy also showed similar results [51]. Larger overlap region increases the possibility of defects recombination during the cascade process, thus reducing the number of residual defects in the system. On the contrary,

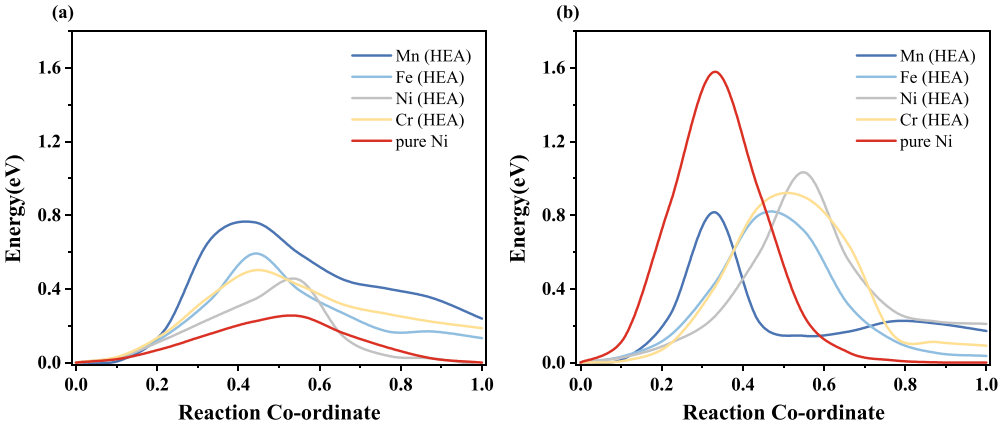

Figure 9. Migration energy of defects in FeMnNiCr and Ni. (a) Interstitial. (b) Vacancy.

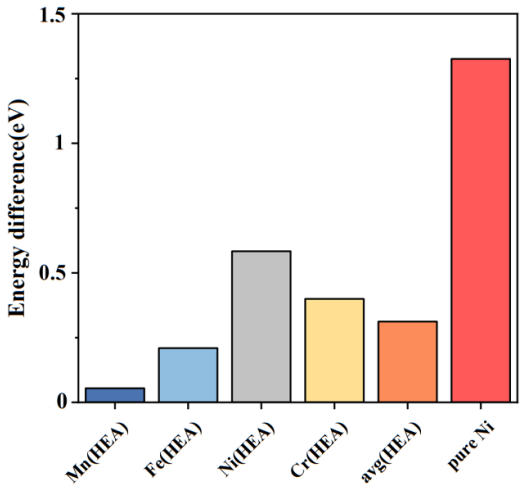

Figure 10. The difference of migration energy between interstitial and vacancy defects in FeMnNiCr and Ni.

the higher migration energy of vacancies in Ni results in accumulation of vacancies in the cascade generation region. While interstitial atoms move farther away, making the encounter and recombination of defects more difficult. Therefore, FeMnNiCr shows superior irradiation resistance due to the higher interstitial migration energy caused by lattice distortion and similar vacancy migration properties.

3.5. Comparison of defects in different HEAs under successive bombardment

In order to compare the irradiation resistance performance between FeMnNiCr and other high-entropy alloys, we also carry out the simulation of different high-entropy alloys with successive bombardment under the same irradiation conditions. The number of model and the temperature are also both kept the same with the simulation systems in section 3.1. The results are displayed in figure 11 for the number of defects in different high-entropy alloys during the

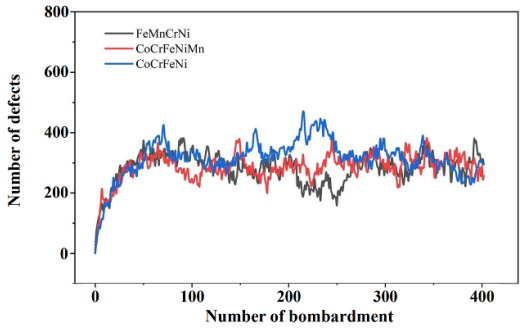

Figure 11. The number of defects in three high-entropy alloys under successive bombardment.

bombardment process. All the three HEAs of FeMnNiCr, CoCrFeNiMn and CoCrFeNi share a similar trend. The number of defects tends to increase at the early stage and saturate and fluctuates dynamically. The number of residual defects in the three high-entropy alloys is also similar at the end of 400 bombardments, which implies FeMnNiCr has similar irradiation resistance performance with other two high-entropy alloys. However, FeMnNiCr is Co-free alloy, which suggests better application potential of FeMnNiCr in the field of nuclear energy.

4. Conclusion

The irradiation resistance behavior of FeMnNiCr under prolonged irradiation conditions has been investigated by means of MDs simulations. The results indicate that the number of defects in FeMnNiCr saturates after about 56 times of bombardments, while that in Ni grows continuously during the bombardment process and eventually significantly exceeds that of FeMnNiCr. Large size interstitial clusters are not observed in FeMnNiCr, and the vacancy defects number with small size clusters are significantly smaller than that of Ni. In addition, the formation and growth of dislocation are significantly inhibited in FeMnNiCr after irradiation, while obvious dislocation appears in Ni.

Vacancy defects tend to form in both two materials after irradiation. The small difference in defect migration energy of FeMnNiCr compared to Ni implies that interstitials and vacancies defects are prone to recombination thus better irradiation resistance in HEAs. Besides, the irradiation resistance performance of FeMnNiCr is similar to that of CoCrFeNiMn and CoCrFeNi. FeMnNiCr has extra advantage in nuclear area application due to the absence of Co which is harmful in nuclear energy application. Therefore, our results suggest that FeMnNiCr can be an excellent candidate for nuclear structural material.

Data availability statement

The data cannot be made publicly available upon publication because they are not available in a format that is sufficiently accessible or reusable by other researchers. The data that support the findings of this study are available upon reasonable request from the authors.

Acknowledgment

The work is supported by the Fundamental Research Funds for the Central Universities (No. FRF-IDRY-20-008). Q. P. would like to acknowledge the support provided by National Natural Science Foundation of China (Grant No. 12272378), Strategic Priority Research Program of Chinese Academy of Sciences (Grant No. XDB0620103) and High-level Innovation Research Institute Program of Guangdong Province (Grant No. 2020B0909010003).

Conflict of interest

The authors declare that they have no known competing financial interests or personal relationships that could have appeared to influence the work reported in this paper.

ORCID iDs

Zunhao Liu https://orcid.org/0009-0009-5174-4775
Rui Li https://orcid.org/0000-0003-0258-281X
Qing Peng https://orcid.org/0000-0003-4122-5380

References

[1] Balbaud F *et al* 2021 A NEA review on innovative structural materials solutions, including advanced manufacturing processes for nuclear applications based on technology readiness assessment *Nucl. Mater. Energy* **27** 101006
[2] Gilbert M R, Arakawa K, Bergstrom Z, Caturla M J, Dudarev S L, Gao F, Goryaeva A M, Hu S Y, Hu X, Kurtz R J and Litnovsky A 2021 Perspectives on multiscale modelling and experiments to accelerate materials development for fusion *J. Nucl. Mater.* **554** 153113
[3] Was G S, Petti D, Ukai S and Zinkle S 2019 Materials for future nuclear energy systems *J. Nucl. Mater.* **527** 151837
[4] Wu Y, Naren M, Wang Q, Wang H and Chen J 2013 The establishment of prophase innovative management system in nuclear power project *Adv. Mater. Res.* **671–674** 3040–3
[5] Zinkle S J and Was G 2013 Materials challenges in nuclear energy *Acta Mater.* **61** 735–58
[6] Yeh J W, Chen S K, Lin S J, Gan J Y, Chin T S, Shun T T, Tsau C-H and Chang S-Y 2004 Nanostructured high-entropy alloys with multiple principal elements: novel alloy design concepts and outcomes *Adv. Eng. Mater.* **6** 299–303
[7] Cantor B, Chang I, Knight P and Vincent A 2004 Microstructural development in equiatomic multicomponent alloys *Mater. Sci. Eng.* **375** 213–8
[8] Liu D *et al* 2022 Exceptional fracture toughness of CrCoNi-based medium- and high-entropy alloys at 20 kelvin *Science* **378** 978–83
[9] Li W, Liaw P K and Gao Y 2018 Fracture resistance of high entropy alloys: a review *Intermetallics* **99** 69–83
[10] Li C, Hu X, Yang T, Kumar N A P K, Wirth B D and Zinkle S J 2019 Neutron irradiation response of a Co-free high entropy alloy *J. Nucl. Mater.* **527** 151838
[11] Chuang M H, Tsai M H, Wang W R, Lin S J and Yeh J W 2011 Microstructure and wear behavior of $Al_xCo_{1.5}CrFeNi_{1.5}Ti_y$ high-entropy alloys *Acta Mater.* **59** 6308–17
[12] Li Y, Li R and Peng Q 2019 Enhanced surface bombardment resistance of the CoNiCrFeMn high entropy alloy under extreme irradiation flux *Nanotechnology* **31** 025703
[13] Su Z, Shi T, Shen H, Jiang L, Wu L, Song M, Li Z, Wang S and Lu C 2022 Radiation-assisted chemical short-range order formation in high-entropy alloys *Scr. Mater.* **212** 114547
[14] Yang L *et al* 2019 High He-ion irradiation resistance of CrMnFeCoNi high-entropy alloy revealed by comparison study with Ni and 304SS *J. Mater. Sci. Technol.* **35** 300–5
[15] Dou Y, Jin K, He X, Yang W, Zhong W, Cao H and Huang C 2019 Research progress on anti-irradiation property of high-entropy alloy *At. Energy Sci. Technol.* **53** 1868

[16] Lu C *et al* 2016 Enhancing radiation tolerance by controlling defect mobility and migration pathways in multicomponent single-phase alloys *Nat. Commun.* **7** 13564
[17] Zhang Y, Jiang W Q, Gokhman A, Yang J J, Shi K, Luan J H, Cui Y, Liaw P K, Liu C T and Zhang Z W 2021 Enhanced irradiation tolerance of $Fe_{30}Cr_{25}Ni_{20}Co_{15}Mn_{10}$ high-entropy alloy via nanotwin boundaries *J. Nucl. Mater.* **557** 153292
[18] Abhaya S, Rajaraman R, Kalavathi S, David C, Panigrahi B K and Amarendra G 2016 Effect of dose and post irradiation annealing in Ni implanted high entropy alloy FeCrCoNi using slow positron beam *J. Alloys Compd.* **669** 117–22
[19] Zhang Y *et al* 2019 Thermal stability and irradiation response of nanocrystalline CoCrCuFeNi high-entropy alloy *Nanotechnology* **30** 294004
[20] Zhao S, Zhang Y and Weber W J 2022 High entropy alloys: irradiation *Encyclopedia of Materials: Metals and Alloys* ed F G Caballero (Elsevier) pp 533–47
[21] Li Y, Li R, Peng Q and Ogata S 2020 Reduction of dislocation, mean free path, and migration barriers using high entropy alloy: insights from the atomistic study of irradiation damage of CoNiCrFeMn *Nanotechnology* **31** 425701
[22] Li R, Li Y, Liu Y and Peng Q 2023 The effect of grain boundary on irradiation resistance of CoCrCuFeNi high entropy alloy *Comput. Mater. Sci.* **225** 112185
[23] Bacon D J, Gao F and Osetsky Y N 2000 The primary damage state in fcc, bcc and hcp metals as seen in molecular dynamics simulations *J. Nucl. Mater.* **276** 1–12
[24] Lin Y, Yang T, Lang L, Shan C, Deng H, Hu W and Gao F 2020 Enhanced radiation tolerance of the Ni-Co-Cr-Fe high-entropy alloy as revealed from primary damage *Acta Mater.* **196** 133–43
[25] Do H-S and Lee B-J 2018 Origin of radiation resistance in multi-principal element alloys *Sci. Rep.* **8** 16015
[26] Ullah M W, Aidhy D S, Zhang Y and Weber W J 2016 Damage accumulation in ion-irradiated Ni-based concentrated solid-solution alloys *Acta Mater.* **109** 17–22
[27] Gao F and Weber W J 2002 Cascade overlap and amorphization in 3 C− SiC: defect accumulation, topological features, and disordering *Phys. Rev.* B **66** 024106
[28] He M R, Wang S, Jin K, Bei H, Yasuda K, Matsumura S, Higashida K and Robertson I M 2016 Enhanced damage resistance and novel defect structure of CrFeCoNi under *in situ* electron irradiation *Scr. Mater.* **125** 5–9
[29] Tuomisto F *et al* 2020 Segregation of Ni at early stages of radiation damage in NiCoFeCr solid solution alloys *Acta Mater.* **196** 44–51
[30] Fan Z, Zhong W, Jin K, Bei H, Osetsky Y N and Zhang Y 2021 Diffusion-mediated chemical concentration variation and void evolution in ion-irradiated NiCoFeCr high-entropy alloy *J. Mater. Res.* **36** 298–310
[31] Wang R, Chen Z, Shu Y, Lin Y, Liu Z, Deng H, Hu W and Yang T 2023 Molecular dynamics simulation of effects of Al on the evolution of displacement cascades in AlxCoCrFeNi high entropy alloys *J. Nucl. Mater.* **577** 154342
[32] Shi T *et al* 2021 Current development of body-centered cubic high-entropy alloys for nuclear applications *Tungsten* **3** 197–217
[33] Kumar N K, Li C, Leonard K, Bei H and Zinkle S 2016 Microstructural stability and mechanical behavior of FeNiMnCr high entropy alloy under ion irradiation *Acta Mater.* **113** 230–44
[34] Wu Z and Bei H 2015 Microstructures and mechanical properties of compositionally complex Co-free $FeNiMnCr_{18}$ FCC solid solution alloy *Mater. Sci. Eng.* **640** 217–24
[35] Fang Q, Peng J, Chen Y, Li L, Feng H, Li J, Jiang C and Liaw P K 2021 Hardening behaviour in the irradiated high entropy alloy *Mech. Mater.* **155** 103744
[36] Dong J, Feng X, Hao X and Kuang W 2021 The environmental degradation behavior of FeNiMnCr high entropy alloy in high temperature hydrogenated water *Scr. Mater.* **204** 114127
[37] Thompson A P *et al* 2022 LAMMPS—a flexible simulation tool for particle-based materials modeling at the atomic, meso, and continuum scales *Comput. Phys. Commun.* **271** 108171
[38] Choi W-M, Jo Y H, Sohn S S, Lee S and Lee B-J 2018 Understanding the physical metallurgy of the CoCrFeMnNi high-entropy alloy: an atomistic simulation study *NPJ Comput. Mater.* **4** 1
[39] Ziegler J F and Biersack J P 1985 The stopping and range of ions in matter *Treatise on Heavy-Ion Science: Volume 6: Astrophysics, Chemistry, and Condensed Matter* ed D A Bromley (Springer) pp 93–129
[40] Stukowski A 2012 Structure identification methods for atomistic simulations of crystalline materials *Modelling Simul. Mat. Sci. Eng.* **20** 045021

[41] Nordlund K, Ghaly M, Averback R, Caturla M, de La Rubia T D and Tarus J 1998 Defect production in collision cascades in elemental semiconductors and fcc metals *Phys. Rev.* B **57** 7556
[42] Stukowski A, Bulatov V V and Arsenlis A 2012 Automated identification and indexing of dislocations in crystal interfaces *Model. Simul. Mat. Sci. Eng.* **20** 085007
[43] Faken D and Jónsson H 1994 Systematic analysis of local atomic structure combined with 3D computer graphics *Comput. Mater. Sci* **2** 279–86
[44] Li R, Guo L, Liu Y, Xu Q and Peng Q 2023 Irradiation resistance of CoCrCuFeNi high entropy alloy under successive bombardment *Acta Metall. Sin.* **36** 1482–92
[45] Levo E, Granberg F, Fridlund C, Nordlund K and Djurabekova F 2017 Radiation damage buildup and dislocation evolution in Ni and equiatomic multicomponent Ni-based alloys *J. Nucl. Mater.* **490** 323–32
[46] Guan H, Huang S, Ding J, Tian F, Xu Q and Zhao J 2020 Chemical environment and magnetic moment effects on point defect formations in CoCrNi-based concentrated solid-solution alloys *Acta Mater.* **187** 122–34
[47] Zhao S, Egami T, Stocks G M and Zhang Y 2018 Effect of d electrons on defect properties in equiatomic NiCoCr and NiCoFeCr concentrated solid solution alloys *Phys. Rev. Mater.* **2** 013602
[48] Wang C H, Guo L, Li R and Peng Q 2024 Atomistic insights into the irradiation resistance of co-free high entropy alloy FeMnNiCr *Acta Metall. Sinica* **37** 1657–66
[49] Henkelman G, Uberuaga B P and Jónsson H 2000 A climbing image nudged elastic band method for finding saddle points and minimum energy paths *J. Chem. Phys.* **113** 9901–4
[50] Maras E, Trushin O, Stukowski A, Ala-Nissila T and Jonsson H 2016 Global transition path search for dislocation formation in Ge on Si (001) *Comput. Phys. Commun.* **205** 13–21
[51] Li T X, Miao J-W, Guo E Y, Huang H, Wang J, Lu Y P, Wang T-M, Cao Z-Q and Li T-J 2021 Tungsten-containing high-entropy alloys: a focused review of manufacturing routes, phase selection, mechanical properties, and irradiation resistance properties *Tungsten* **3** 181–96